HOSTED BY

ELSEVIER

Available online at www.sciencedirect.com

ScienceDirect

Soils and Foundations 59 (2019) 2206–2219

www.elsevier.com/locate/sandf

Technical Paper

Bearing capacity of composite ground with soil-cement columns under earth fills: Physical and numerical modeling

Pengpeng Ni [a,b], Yaolin Yi [b,*], Songyu Liu [c]

[a] Southern Marine Science and Engineering Guangdong Laboratory (Zhuhai), Guangdong Key Laboratory of Oceanic Civil Engineering, Guangdong Research Center for Underground Space Exploitation Technology, School of Civil Engineering, Sun Yat-sen University, Guangzhou 510275, China
[b] School of Civil and Environmental Engineering, Nanyang Technological University, Singapore 639798, Singapore
[c] Institute of Geotechnical Engineering, Southeast University, Nanjing 210096, China

Received 9 May 2019; received in revised form 3 December 2019; accepted 17 December 2019
Available online 1 February 2020

Abstract

Soil-cement columns are widely used to improve soft ground, and the bearing capacity of the formed composite ground is a key design parameter. The currently employed design method was developed for composite grounds under rigid footings, whilst the bearing capacity behavior of composite grounds under earth fills with different degrees of stiffness has rarely been investigated. Hence, the present study attempts to fill this gap. In this investigation, 1-g laboratory model tests are conducted to compare the bearing capacity behavior of composite grounds under a rigid footing and under embankment fill, based on which a numerical model that can capture the strain-softening behavior of soil-cement columns is established. The calibrated numerical model is further employed to perform 144 analyses. The results indicate that the failure mode of composite grounds differs for different types of earth fills: soil failure occurs prior to column failure under soft clay and dredged slurry, whereas column failure is the primary failure mode for composite grounds under embankment fill. This difference in failure mode of composite grounds can be explained using soil arching theories. For different failure modes, different bearing capacity efficiency factors should be used in design.

Keywords: Composite ground; Soil-cement column; Earth fills; Bearing capacity; Failure mode

1. Introduction

Soil-cement columns are increasingly being used worldwide to improve the bearing capacity of soft grounds; they can be installed through either deep mixing (Shen et al., 2003, 2008; Kitazume and Terashi, 2013; Chai et al., 2017; Yi et al., 2019) or jet grouting (Shen et al., 2013, 2017; Wang et al., 2019). The deep mixing technique uses blades/augers to mechanically mix cement slurry (or powder) with soil, while the jet grouting method pumps cement slurry at a high pressure to cut soil for mixing. Hence, deep mixing columns are less heterogeneous than jet grouting columns, and are widely used for common sites, whereas jet grouting columns are used for constrained sites, e.g., excavation pits and below bridges/electrical cables.

In design, it is critical to estimate the ultimate bearing capacity of a composite ground (q_{cs}) with soil-cement columns, which is mainly dominated by the ultimate bearing capacities of a single column (q_c) and the untreated ground (q_s), as well as the area replacement ratio (m = area of the column / area of the improved zone). For example, as recommended in the design guidelines in China (JGJ 79, 2012), Eq. (1) can be used to evaluate the bearing capacity of a composite ground, q_{cs}, for different types of columns,

Peer review under responsibility of The Japanese Geotechnical Society.
* Corresponding author.
E-mail address: yiyaolin@ntu.edu.sg (Y. Yi).

https://doi.org/10.1016/j.sandf.2019.12.004
0038-0806/

where q_c and q_s are superimposed by different fractions through m, and there are two bearing capacity efficiency factors for the column (λ) and the soil between columns (β). Since the failure strain of soil is often much higher than that of cement-stabilized soil (Lorenzo and Bergado, 2006), i.e., brittle column failure occurs prior to ductile soil failure, the bearing capacity of an untreated ground cannot be fully mobilized for a composite ground (i.e., $\beta < 1.0$). Therefore, for a composite ground with soil-cement columns, JGJ 79 (2012) suggests a λ value of 1.0, assuming that the bearing capacity of the column is fully mobilized, and a β value of 0.1 to 0.8, depending on the soil type. For fully penetrating uniform long soil-cement columns in soft soils, q_c is usually governed by the unconfined compressive strength of the column (q_u). As such, Eq. (1) can be replaced by Eq. (2) (Yi et al., 2018).

$$q_{cs} = \lambda m q_c + \beta(1-m)q_s \tag{1}$$

$$q_{cs} = m q_u + \beta(1-m)q_s \tag{2}$$

However, the above-mentioned design method was developed based on the experience of using a composite ground under a rigid (e.g., concrete) footing with or without a thin sand/gravel cushion (Fig. 1a). The behavior of composite grounds under earth fills is different from that of composite grounds under rigid footings. Under a rigid footing, a negligible differential settlement between the soil and the column could occur and the stress mobilization of the composite ground could be dominated by the column settlement, whilst under earth fills, the settlement of the soil could be much higher than the settlement of the column (Bergado and Lorenzo, 2002; Rowe and Liu, 2015; Yi et al., 2016; King et al., 2017). Although the settlement behavior of a composite ground with soil-cement columns under earth fills, especially under embankments, has been widely studied, the bearing capacity behavior has rarely been investigated. Wu (2000) conducted two model-scale tests on composite grounds with soil-cement columns, 120 mm in diameter and 2 m in length, in soft clays with an m value of 15%, and found that the failure modes of the composite ground under a rigid footing and under earth fills were controlled by column failure and soil failure, respectively. Based on the results of Wu (2000), Gong (2007) suggested that soil failure could occur prior to column failure for composite grounds under a flexible foundation (e.g., embankment fill), leading to $\beta = 1.0$ and $\lambda < 1.0$ in Eq. (1); and hence, the bearing capacity of a composite ground under earth fills could be lower than that under a rigid footing. Nevertheless, to the authors' best knowledge, the work of Wu (2000) is the only study in which the bearing capacity of composite foundations under earth fills has been investigated. Furthermore, the effect of earth fills on the bearing capacity of composite grounds with soil-cement columns has not been considered in any design codes. Additionally, different types of earth fills could have different levels of strength and stiffness, affecting the bearing capacity of composite grounds with soil-cement columns. For example, a compacted embankment fill (Fig. 1b), with a friction angle of 30° to 40°, typically has much higher levels of shear strength and stiffness than an excavated clay lump (soft clay in Fig. 1c), with an undrained shear strength (c_u) of less than 20 kPa, or dredged slurry (Fig. 1d, close to an ideal flexible pressure), with a negligible c_u. The influence of earth fills on the bearing capacity of composite grounds with soil-cement columns and its effect on practical design (e.g., the values of λ and β in Eq. (1)) need to be comprehensively investigated; and thus, they are the main objectives of this study.

It is noted that a load transfer platform (LTP), consisting of granular materials and/or geosynthetic reinforcement, can be set at the bottom of the embankment fill to facilitate the load transfer from the embankment to the piles or the columns (Han and Gabr, 2002). In Japan, the load transferred slab (LTS) has been reported for use in soil-cement column-supported embankments (Shen et al., 2001), and has a similar function to that of the LTP in rigid pile-supported embankments. The LTS is a soil-cement slab with a thickness of about 1 m that is installed using the shallow mixing method. If a LTP or LTS is used for a composite ground under embankment fill (Fig. 1b), soft clay (Fig. 1c) or dredged slurry (Fig. 1d), the stiffness of the earth fill will be between the case under a rigid footing (Fig. 1a) and that under embankment fill (Fig. 1b). In this study, the use of LTP/LTS is not considered.

In this investigation, the techniques of 1-g laboratory physical modeling and numerical modeling are adopted

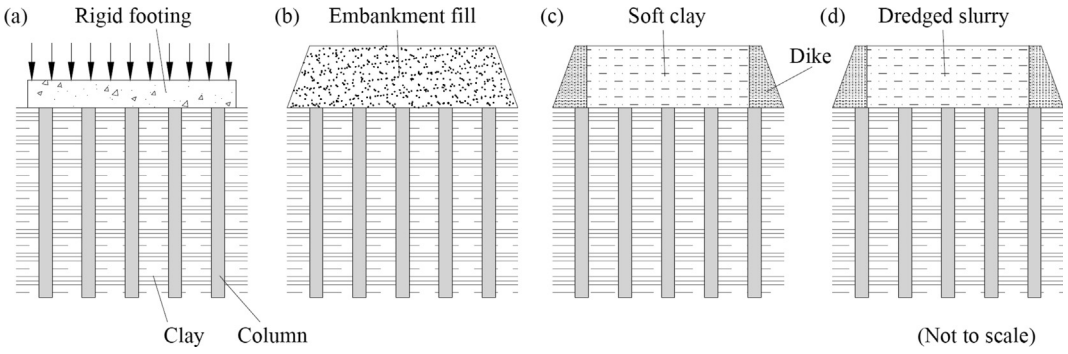

Fig. 1. Composite grounds under (a) rigid footing, (b) embankment fill, (c) soft clay, and (d) dredged slurry.

to analyze the bearing capacity of composite grounds with soil-cement columns under earth fills. In the laboratory modeling, the bearing capacity behavior of composite grounds under a rigid footing and under embankment fill is compared. The experimentally measured stress-settlement curves are used to calibrate a numerical model with the capability of simulating the strain-softening behavior of soil-cement columns. A parametric study of 144 analyses is then conducted to investigate the bearing capacity of composite grounds with soil-cement columns under different types of earth fills (Fig. 1). The difference in failure mechanism of composite grounds due to the different types of earth fills is explained through soil arching models, and the calculated soil arching ratios are compared against analytical solutions. In the end, the bearing capacity efficiency factors for the column and the soil are calculated for different scenarios.

2. 1-g laboratory physical modeling

2.1. Experimental program

2.1.1. Test chamber

The 1-g physical modeling was employed to compare the bearing capacity behavior of composite grounds under a rigid footing and under embankment fill (Fig. 1a and b). The cases under soft clay and dredged slurry (Fig. 1c and d) were not conducted, since it was very hard to model them in the laboratory. According to the similitude laws, all dimensions were scaled by a factor of 1:10 in the laboratory tests. Due to the limitation of the 1-g laboratory physical modeling (i.e., the prototype stress field cannot be reproduced with a small-scale model), the elevation of the earth fill was not simulated directly. Instead, a loading plate was used above a sand cushion to apply vertical stress to simulate the effect of overburden pressure above the composite ground. The rigid footing was simulated with a loading plate acting above a 2-cm sand cushion (Fig. 2a) to facilitate the installation of measurement sensors, whereas the embankment fill was simulated with a loading plate acting above a 20-cm sand cushion (Fig. 2b). Yi et al. (2016) demonstrated that a 20-cm-thick sand cushion could produce an adequate level of differential settlement between the soil and the column in model tests with a scale factor of 1:10.

As shown in Fig. 2, the model column had a diameter of 5 cm and a length of 60 cm. The column length was equivalent to the thickness of the soft clay, simulating fully penetrating columns. The spacing between the soil-cement columns is a site-specific parameter, falling within the range of 1.0 m to 2.2 m (Liu et al., 2012; Ye et al., 2012). In general, the area replacement ratio varies from 8% to 20% in China (Yi et al., 2016). According to JGJ 79 (2012), the bearing capacity of a composite ground can be determined by a plate loading test on a single-column composite ground or a multiple-column composite ground. For the model test in this study, the single-column composite ground was used in order to reduce the total loading area as well as the size of the test chamber. The loading plate was manufactured using stainless acrylic with a thickness of 2 cm and a diameter of 16 cm, and the soil below the loading plate contributed to the bearing capacity of the composite ground. Hence, the area replacement ratio, the m value, was calculated as 10% in the test, falling within the common range used in practice. Axial loads were applied on the loading plate by dead weights through a mechanical lever system. Silicon grease was applied at all boundaries to minimize the influence of the interface friction.

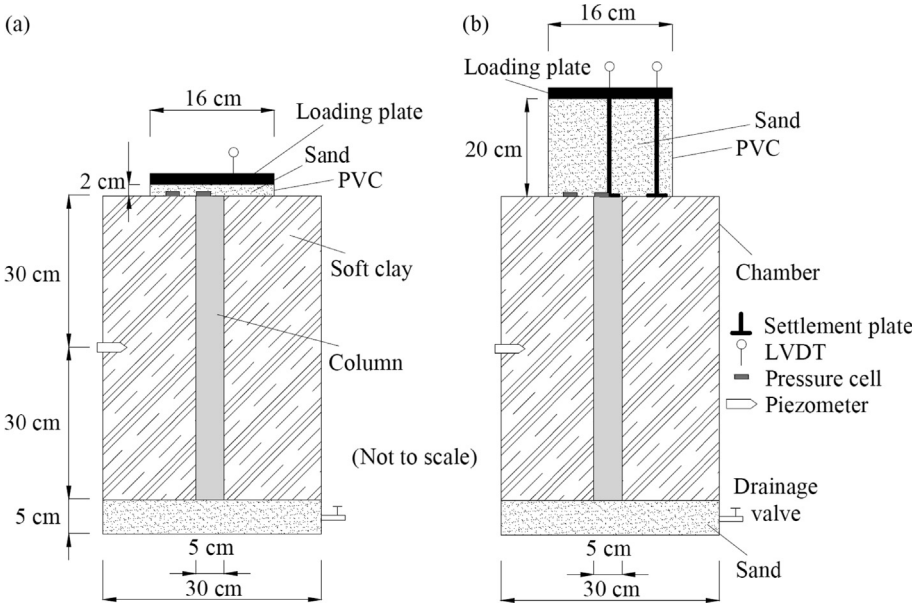

Fig. 2. Schematics of composite grounds under (a) rigid footing and (b) embankment fill.

2.1.2. Materials

The soft clay had plastic and liquid limits of 33% and 74%, respectively. The sand above and below the soft clay was poorly graded, with $d_{10} = 0.15$ mm, $d_{30} = 0.2$ mm, $d_{60} = 0.4$ mm, a uniformity coefficient of $C_u = 2.67$, and a coefficient of gradation of $C_c = 0.67$. The bearing stratum of sand was firstly poured into the chamber. A surcharge pressure of 96 kPa was applied on the sand until no settlement was observed. The soft clay was mixed with water at a water content of 110%, after which the clay-water slurry was poured into the chamber. Pre-consolidation with a surcharge of 24 kPa was conducted for the clay slurry, during which the drainage valve was open. When the excess pore water pressure measured from the piezometer (Fig. 2) became less than 4 kPa, the pre-consolidation was terminated. A miniature vane shear apparatus was used to measure the undrained shear strength (c_u) of the soft clay at three depths, showing a variation of 11 kPa (top), 7 kPa (middle), and 9 kPa (bottom). The binder consisted of 80% ground granulated blast-furnace slag (GGBS) and 20% reactive magnesia (MgO) in a dry binder content of 30%, which was determined according to Yi et al. (2014). The binder was mixed with the soft clay at a water content of 110% to produce the slurry-form mixture, which was cured in an auger-drilled hole with a diameter of 5 cm for 28 days. Details of the column installation procedure have been published by Yi et al. (2016).

2.1.3. Instrumentation

As depicted in Fig. 2, a miniature piezometer was installed at the mid-height of the clay to monitor the pre-consolidation process. Miniature earth pressure cells were employed to record the vertical stresses on top of the column and the clay. Linear variable displacement transducers (LVDTs) were mounted with settlement plates to measure the settlement of the column and the clay. The loading plate was drilled with holes to facilitate the contact between settlement plate and LVDT. In the test under the rigid footing, there was only one LVDT set on the loading plate. Readings from all sensors were digitalized and monitored through a data logger, which recorded the values at 1 min intervals.

2.1.4. Test scheme

The loading procedure was adopted following the JGJ 79 (2012) design guidelines. The load increment was 10.6 kPa for a maintaining duration of 2 h. The drainage valve was closed during the loading test to simulate the undrained condition. Two criteria were employed for determining the time to terminate the test: (a) the measured settlement in the current loading step exceeded the settlement in the previous step by five times, or (b) the current settlement was more than two times the previous settlement, but it could not reach stability after 24 h. Once the failure was identified, the applied load prior to failure was denoted as the ultimate bearing capacity of the composite ground, q_{cs}.

Excavation was implemented to extrude the column after the loading test to observe the failure pattern of the column. Furthermore, the column was cut for unconfined compressive strength (i.e., q_u) tests. For the column under rigid footing, the measured strength values were 459 kPa and 549 kPa, with an average of 504 kPa. The strength values for the column under embankment fill were 437 kPa and 409 kPa, with an average of 423 kPa. The average strength of the column under rigid footing was higher (i.e., 81 kPa) than the average strength of the column under embankment fill, the difference of which could have been induced during the installation process, including borehole drilling, pouring the slurry-form mixture, and compaction.

2.2. Experimental results

Fig. 3 presents the applied stress-settlement curves for the two composite ground tests. The soil and the column are assumed to settle equally under the loading plate in the composite ground under rigid footing; and hence, a single applied stress-settlement curve is obtained for this case. As expected, a significant differential settlement between the soil and the column is measured in the composite ground test under embankment fill. All three stress-settlement curves show a linear pattern at the initial loading stage, after which a sudden increase in settlement is observed. Hence, the ultimate bearing capacities can be easily identified, namely, 127.3 kPa and 116.7 kPa for the composite ground under rigid footing and under embankment fill, respectively. As mentioned previously, the average strength of a column under rigid footing is 81 kPa more than that under embankment fill, which could be responsible for the slightly higher bearing capacity of composite ground under rigid footing.

Variations in the measured stresses with time for the two composite grounds are illustrated in Fig. 4. The measured soil and column stresses were used to back-calculate the

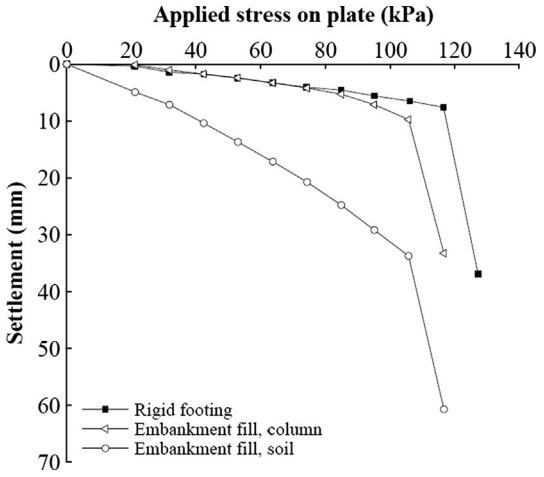

Fig. 3. Stress-settlement curves for composite grounds under rigid footing and embankment fill.

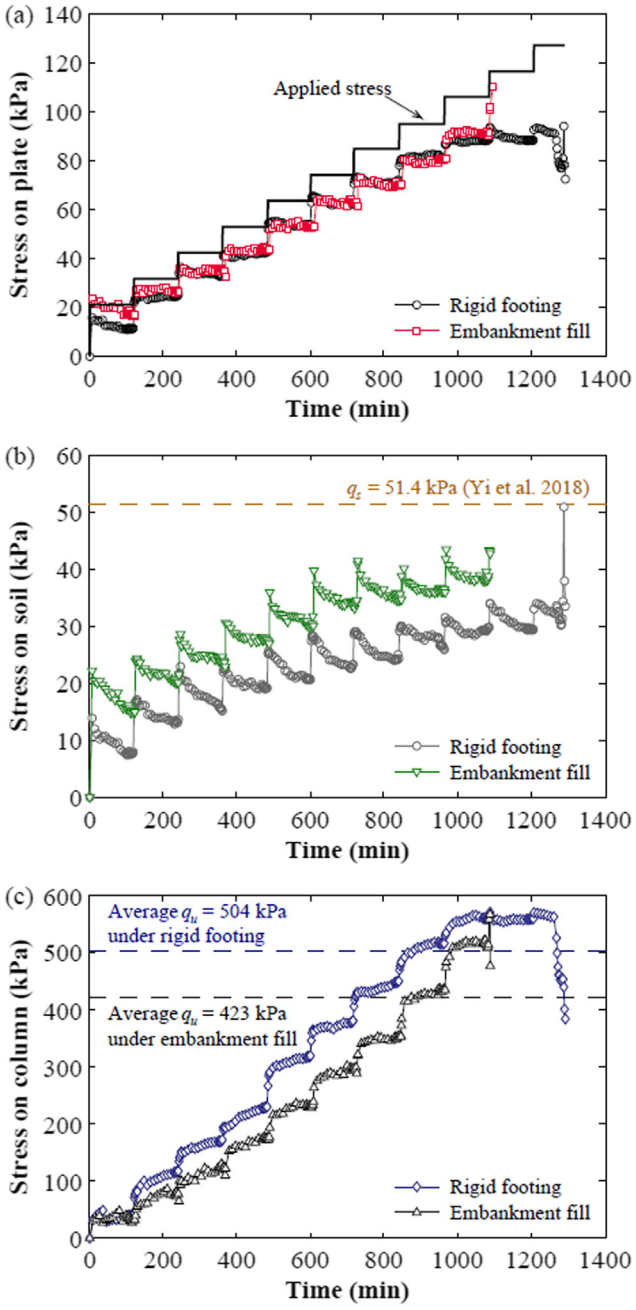

Fig. 4. Variations in measured stresses for composite grounds with time: (a) on the plate, (b) on the soil, and (c) on the column.

applied stress on the plate based on the area replacement ratio. Fig. 4a shows that the back-calculated and the applied stresses on the plate for the two tests are generally consistent. In Fig. 4b and c, it can be seen that both the soil and column stresses increase instantaneously upon the application of a new stress increment. During the maintaining period of 2 h, the soil stress decreases and the column stress increases, demonstrating that load transfer occurs in the soil-column system. As observed in previous studies (Horpibulsuk et al., 2012; Yi et al., 2016), the occurrence of load transfer from the soil to the column accelerates the dissipation of excess pore water pressure in the soil. Prior to the failure of the composite ground, the measured soil stress in Fig. 4b never exceeds the ultimate bearing capacity of the untreated ground of 51.4 kPa, which was measured by Yi et al. (2018) for the same soil. Column failure is observed prior to soil failure in both composite grounds, with the evidence that the measured column stress exceeds the average column strength, q_u, first. The measured column stress is higher than the column strength. This is because, firstly, the pressure cell was placed in the center of the column top, where the stress was the highest, and the inclusion of a relatively rigid pressure cell caused the arching effect, i.e., stress concentration (Talesnick, 2013); secondly, the column strength was tested on the column specimens after the failure of the composite ground, and the applied load could have caused some deteriorations in the column. Nevertheless, according to Fig. 4a, the measured stresses are generally reliable. With the last load increment, the drop in column stress and the sudden increase in soil stress demonstrate the occurrence of column failure, and the applied load is then transferred to the surrounding soil, inducing soil failure. When the ultimate bearing capacity of the composite ground is mobilized, the column strength is fully utilized (i.e., λ can be considered as 1.0). For the composite ground under rigid footing, the column and the soil settle together, and the soil strength is not fully mobilized, leading to $\beta = 0.61$ at the ultimate bearing capacity of the composite ground. For the composite ground under embankment fill, the soil stress can transfer to the column before the occurrence of column failure. Hence, soil failure does not occur prior to column failure, and the bearing capacity efficiency factor for soil is calculated as $\beta = 0.74$ at q_{cs}.

Fig. 5 shows the soil/column stress-settlement curves for the two composite grounds in this study, as well as those of an untreated ground (Yi et al., 2018) and a single column (Yi et al., 2017) with the same soil and column. It is evident that the three column stress-settlement curves are very similar, indicating that the column under the three different conditions fails in the same way. However, the three soil

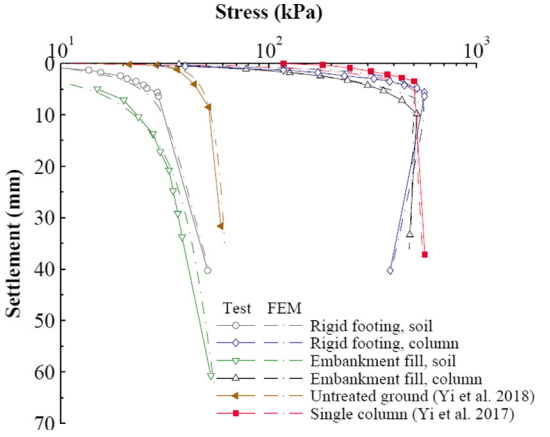

Fig. 5. Stress-settlement curves obtained from model-scale laboratory tests and finite element analyses.

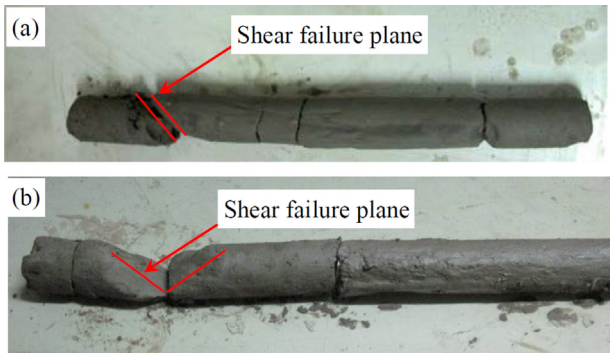

Fig. 6. Photos of excavated columns: (a) failed column under rigid footing and (b) failed column under embankment fill.

stress-settlement curves in Fig. 5 are quite different. Upon the occurrence of failure in the composite ground, i.e., q_{cs}, the column stress in the composite ground tests exceeds the column strength, q_u, while the soil stress is always less than the ultimate bearing capacity of the untreated ground, q_s. This indicates that column failure occurs before soil failure for both composite grounds.

Fig. 6 presents photos of extruded columns, where an inclined shear failure plane can be clearly observed in each column. It is noted that some horizontal fractures are introduced into the columns during the excavation. The shear failure plane in each column initiates at a depth of approximately 100 mm below the column head, which is similar to the failure pattern observed in the single column test (Yi et al., 2017). This confirms that the columns under rigid footing and under embankment fill have the same failure patterns.

Although the composite grounds under rigid footing and embankment fill (Fig. 1a and 1b) show some differences in settlement and load transfer mechanism, their failure modes are the same, the viewpoint of which is contrary to that of Wu (2000). However, it should be emphasized that the embankment fill was modeled with a 20-cm-thick sand cushion and the load was applied on a loading plate above the cushion, which could have affected the failure mode. Additionally, it is very hard to conduct tests for composite grounds under soft clay and dredged slurry (Fig. 1c and d) through 1-g physical modeling. Hence, a numerical simulation is performed to compare the bearing behavior of composite grounds under all four conditions as shown in Fig. 1.

3. 3D numerical modeling

3.1. Calibration of numerical model

3.1.1. Constitutive model

In the current study, the short-term response of a composite ground with soil-cement columns was simulated following the undrained condition. It was assumed that the groundwater level was at the ground surface and the subsoils were fully saturated, leading to a short-term friction angle of zero in the total stress framework. It has been demonstrated that the standard Mohr-Coulomb model can be used to simulate subsoils by assigning a friction angle of zero and a cohesion of undrained shear strength to provide a reliable short-term analysis for column-supported embankments (Abusharar et al., 2009; Voottipruex et al., 2011; Jamsawang et al., 2015); and hence, the same modeling strategy was also adopted in this analysis.

The stress-strain response of cement-stabilized soil generally shows a brittle failure pattern with a linear behavior up to the peak strength and a nonlinear softening behavior with the increase in plastic strain under the undrained condition (Lorenzo and Bergado, 2006). Simple constitutive models (e.g., elasto-plastic model) are often incapable of reproducing the strain-softening character, such that a numerical analysis cannot simulate the brittle failure behavior of soil-cement columns correctly. Considering its simplicity, the extended Mohr-Coulomb model (Yapage et al., 2014, 2015) was employed in this investigation to simulate the behavior of soil-cement columns.

As shown in Fig. 7, Horpibulsuk et al. (2004) have revealed that the influence of the confining stress on the response of cemented soils under consolidation pressure can be disregarded, since the cementation bond dominates the strength character. In other words, the undrained stress-strain curves for cemented soils at different confining stresses do not differ much (Lorenzo and Bergado, 2006; Xiao et al., 2014). Therefore, the strain softening behavior of soil-cement columns was modeled by assigning three segmented cohesion intercepts as a function of deviatoric plastic shear strains in this study. Yapage et al. (2015) suggested to use the peak plastic shear strain of 1–4%, the residual plastic shear strain of 4–15%, and the residual softening index of 0.4 to 0.7 based on the results of consolidated undrained triaxial tests on stabilized soil with a cement content of 6–30%. In this study, the lower bound of the residual softening index of 0.4 was used to interpret the strain-softening behavior following the suggestion of

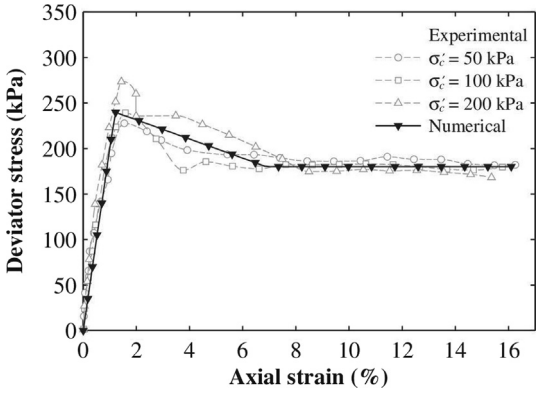

Fig. 7. Comparison of deviator stress versus axial strain curves obtained from consolidated undrained triaxial tests of Horpibulsuk et al. (2004) and numerical simulations.

Table 1
Interpreted shear strength parameters for cemented soil based on consolidated undrained triaxial test results of Horpibulsuk et al. (2004).

Cement content (%)	Elastic modulus, E (MPa)	Peak strength	Strain softening			
		Cohesion, $c_{col,\ p}$ (kPa)	Cohesion, $c_{col,1}$ (kPa)	Plastic strain, ε_1 (%)	Cohesion, $c_{col,2}$ (kPa)	Plastic strain, ε_2 (%)
9	20	120	90	6	90	15

Yapage et al. (2015). To demonstrate the effectiveness of the extended Mohr-Coulomb model in simulating the response of soil-cement columns, the measured stress-strain curves by Horpibulsuk et al. (2004) were modeled for comparison. All derived input parameters for this simulation are tabulated in Table 1. Comparisons of the stress-strain curves obtained from the experimental measurements and the numerical calculations are plotted in Fig. 7. It is proved that the extended Mohr-Coulomb model can effectively reproduce the experimental data regardless of the confining stress, σ_c'.

3.1.2. Input parameters

In the following, the data from plate loading tests on the two composite grounds in this study, as well as the untreated ground (Yi et al., 2018) and the single-column ground (Yi et al., 2017) were used to calibrate the numerical model. In the numerical analysis, the soft clay was simulated under the undrained condition in the total stress framework. For simplicity, the variation in c_u was not considered, and a constant c_u of 11 kPa measured at a shallow depth was used for the soft clay, which mostly affected the bearing behavior of the ground with a small loading area. The undrained Young's modulus of clay is usually calculated by scaling the undrained shear strength with a factor varying from 100 for very soft clay to 1500 for very stiff clay (Das, 2010). In the present study, the constrained modulus of clay was estimated as 1.5 MPa, and the Poisson's ratio was taken as 0.49 to simulate the undrained condition. Since dry sand was used as the embankment fill, it was simulated in the effective stress framework. In this study, the mechanical properties of the sand cushion were not measured. Due to the similarity, the soil parameters of Zhuang and Wang (2018) were adopted to simulate the sand cushion using the standard Mohr-Coulomb model with an elastic modulus of 20 MPa, an effective friction angle of 35°, and a cohesion of 5 kPa. For soil-cement columns, the elastic modulus can be calculated based on a linear correlation with a column strength in the range of $E_{50} = 30\text{–}300 \cdot q_u$ (Lorenzo and Bergado, 2006; Abusharar et al., 2009; Voottipruex et al., 2011; Yapage et al., 2014). Based on the unconfined compressive strength test results, the relation of $E_{50} = 100 \cdot q_u$ was determined in this analysis, and the undrained shear strength of the column was derived using the form of $c_{col} = 0.5 \cdot q_u$ (Yapage et al., 2014; Chai et al., 2015). The Poisson's ratio of the column was taken as 0.2, which falls within the suggested range of 0.1–0.3 by Han et al. (2007) and Yapage et al. (2014).

3.1.3. Model setup and comparison

The responses of the untreated, the single-column, and the composite grounds under rigid footing and embankment fill were simulated by the general-purpose finite element program ABAQUS. The exact same geometries used in the model-scale tests were adopted in the numerical model. All the soil and column elements were characterized using 8-node hexahedral continuum elements. All the lateral boundaries were simulated as smooth and rigid boundaries, where the displacement in the normal direction was constrained. A contact approach was used to capture the sliding phenomenon at the soil-column interface. A sensitivity study was conducted to assess whether the axial loading response of the composite ground could be altered by the definition of the friction coefficient at the soil-column interface. It was found that the results were insensitive to the interface friction coefficient when it varied from 0.2 to 0.5. The value of the interface friction coefficient was taken as 0.2 in the following analyses considering computational efficiency. Axial loads were applied on the loading plate following the test scheme as depicted in Fig. 4a.

The calculated soil/column stress-settlement curves in the numerical model for the untreated, single-column, and composite grounds are compared with those measured in the laboratory in Fig. 5. In general, the two methods provide comparable results. The numerical simulations also show that the influence of the foundation/earth fills on the bearing behavior of the composite grounds with soil-cement columns is negligible in terms of the governing failure mode (column failure occurs prior to soil failure) and the ultimate bearing capacity.

3.2. Parametric study

3.2.1. Analysis scheme

Upon the successful calibration of the numerical model, a parametric study was carried out on composite grounds under a rigid footing and under three types of earth fills (Fig. 1). The embankment fill (Fig. 1b) is often compacted at the optimum water content and is above the groundwater level at the ground surface; therefore, it was simulated in the effective stress framework. The parameters for the embankment fill (Fig. 1b) adopted by different researchers are tabulated in Table 2, based on which three types of embankment fill were simulated in this study, as shown

Table 2
Effective shear strength parameters for embankment fill by different researchers.

Unit weight, γ (kN/m^3)	Elastic modulus, E (MPa)	Poisson's ratio, v (–)	Effective friction angle, ϕ' (°)	Cohesion, c' (kPa)	Reference
20	8	0.3	30	1	Abusharar et al. (2009)
19	1	0.3–0.4	35	20	Chai et al. (2015)
20	7.5	0.33	29	1	Jamsawang et al. (2015)
20	20, 40	0.33	32, 38	5	Huang and Han (2009)
19.1	50	0.3	36.6	17.3	Nunez et al. (2013)
18.5	20	0.3	30	10	Rowe and Liu (2015)
20	40	0.3	35	1	Yu et al. (2016)
17	25	0.2	30	1	Zhuang et al. (2012)
17	25, 40, 50	0.2	30, 35, 40	1, 5, 10	Zhuang and Wang (2018)

Table 3
Parameters for rigid footing and different types of earth fills in parametric study.

Type	Unit weight, γ (kN/m^3)	Elastic modulus, E (MPa)	Poisson's ratio, v (–)	Friction angle (°)	Cohesion (kPa)
Rigid footing	/	210,000	0.15	/	/
Embankment fill 1	20	10	0.3	30	1
Embankment fill 2	20	20	0.3	35	5
Embankment fill 3	20	40	0.3	40	10
Rigid	/	210,000	0.15	/	/
Soft clay	15	1.5	0.2	0	10
Pressure	/	/	/	/	/

Note: The shear strength parameters refer to the effective stress and the total stress parameters for the embankment fill and the soft clay, respectively.

in Table 3. The case of soft clay simulates excavated clay lumps placed above the composite ground (Fig. 1c), where the soft clay was saturated, and hence, was simulated in the total stress framework with an undrained shear strength of 10 kPa. The case of dredged slurry (Fig. 1d) was simulated using ideal flexible pressure. The mechanical parameters of rigid footing and different types of earth fills are summarized in Table 3.

Table 4 lists all the variables for the composite grounds in the parametric study. The column diameter was fixed at $D = 0.5$ m. The area replacement ratio often falls within a range of 8% to 20% (Yi et al., 2016), and the column spacing varies from 1.0 m to 2.2 m (Liu et al., 2012; Ye et al., 2012). Four column spacings were selected as 2.0 m, 1.4 m, 1.2 m, and 1 m, corresponding to the four representative m values of 4.9%, 10%, 13.6%, and 19.6%, respectively. Soil-cement columns in cohesive soils typically have a strength of $q_u = 0.5$–2 MPa (Bruce, 2001), based on which three column strength values of 0.5 MPa, 1.0 MPa, and 2.0 MPa were selected. The undrained shear strength of natural soft clay generally falls within a limited range of $c_u = 20$–30 kPa (Voottipruex et al., 2011; Liu et al., 2012; Chai et al., 2015). In total, four geometric parameters were defined for the column spacing, in addition to three column strength values, two soil strength values, and six types of foundations/fills, which brought the number of analyses to $4 \times 3 \times 2 \times 6 = 144$.

Table 4
Summary of parameters of composite ground in parametric study.

Parameter	Range
Area replacement ratio, m (%)	4.9, 10.0, 13.6, and 19.6
Column spacing, S (m)	2, 1.4, 1.2, and 1
Column strength, q_u (MPa)	0.5, 1, and 2
Soil strength, c_u (kPa)	20, and 30
Type of foundations/fills	Pressure, soft clay, embankment fill 1, embankment fill 2, embankment fill 3, and rigid footing

In the numerical simulation, four soil-cement columns were placed in a square pattern for the composite ground, as illustrated in Fig. 8. As mentioned earlier, the bearing capacity of a composite ground can be determined by a plate loading test on a single-column composite ground or a multiple-column composite ground (JGJ 79, 2012). For the numerical simulation, the four-column composite ground was used to influence the soil to a greater depth. For single-layer soft clay with uniform columns, the size of the loading plate and the number of columns cannot change the bearing capacity of the composite ground, as long as the area replacement ratio is kept constant.

Fig. 9 demonstrates the mesh discretization for a typical case with a column spacing of $S = 2.0$ m. Due to the symmetry of the problem, one-quarter of the composite ground model was established to minimize the computational cost. In this study, the model size was assigned as five times the loading area. Finer elements were used under the loading area, and courser meshes were employed near the lateral boundaries. Two symmetrical planes were fixed against the displacement normal to the planes, and the displacements in other directions were set free. The construction

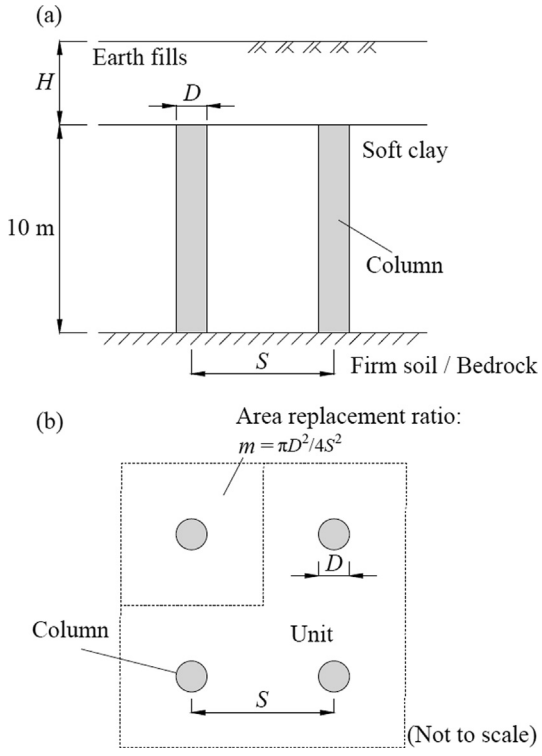

Fig. 8. Schematics of composite ground with four columns: (a) elevation view and (b) plan view.

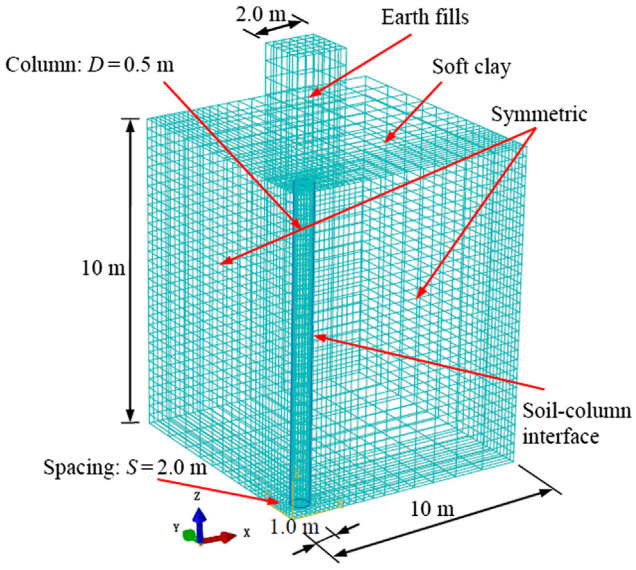

Fig. 9. Finite element discretization of composite ground with four columns under earth fills.

steps for earth fills were explicitly simulated by activating the gravity at different elevations with loading steps.

3.2.2. Results of parametric analysis

The soil/column stress-settlement curves for all the composite grounds can be categorized into three types. Fig. 10 shows an example of the cases with a column spacing of

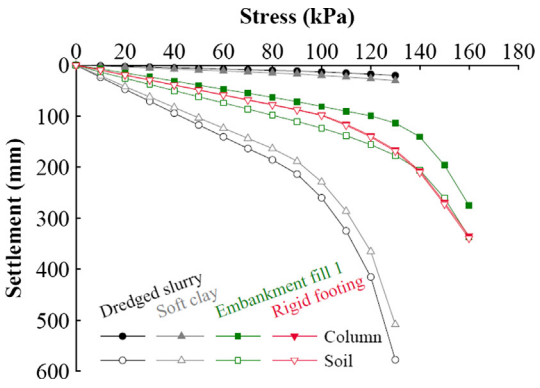

Fig. 10. Stress-settlement curves for composite ground supported by columns with a diameter of $D = 0.5$ m, a spacing of $S = 2.0$ m, and a strength of $q_u = 1.0$ MPa in soft soils with an undrained shear strength of $c_u = 30$ kPa.

$S = 2.0$ m and a strength of $q_u = 1$ MPa in the soft soil with an undrained shear strength of $c_u = 30$ kPa. Under rigid footing, the stress-settlement curves for the soil and the column coincide with each other. Under embankment fill 1, the soil and the column responses differ. This causes differential soil-column settlement, but the stress-settlement curves are similar. Under soft clay or flexible pressure, the stress-settlement curve for the column is linear, while the curve for the soil is nonlinear.

The contours of shear strains in the soil and column were checked carefully to determine the failure modes, i.e., whether column failure or soil failure had occurred first. Examples are shown in Fig. 11 for the cases of the composite grounds under soft clay and embankment fill 1 with a column diameter of $D = 0.5$ m, a spacing of $S = 2.0$ m, and a strength of $q_u = 1.0$ MPa in soft soils with an undrained shear strength of $c_u = 30$ kPa. The term "AC YIELD" (i.e., "actively yielding"), seen in the legend, is an identifier to tell whether or not the material is currently yielding, from which the red zone shows the yielding region. The contours of shear failure for the composite ground under soft clay show that a continuous plastic zone is formed in the soil (Fig. 11a), but yielding does not occur in the column (Fig. 11b) at an applied stress of 120 kPa. For the composite ground under embankment fill 1, a continuous plastic zone is firstly observed in the column (Fig. 11d) at an applied stress of 140 kPa, but the shear band in the soil is not continuous (Fig. 11c). The shear zones develop further with an increase in the fill height. Eventually, excessive shear displacement can be seen in the column at an applied stress of 160 kPa, at which continuous shear planes are formed in both the soil (Fig. 11e) and the column (Fig. 11f). After analyzing all 144 cases, the failure modes of the composite grounds are categorized into two types: (a) soil failure dominates the response of the composite ground under soft clay or ideal flexible pressure, i.e., soil failure occurs before column failure, and (b) the behavior of the composite ground is governed by column failure rather than soil failure for the

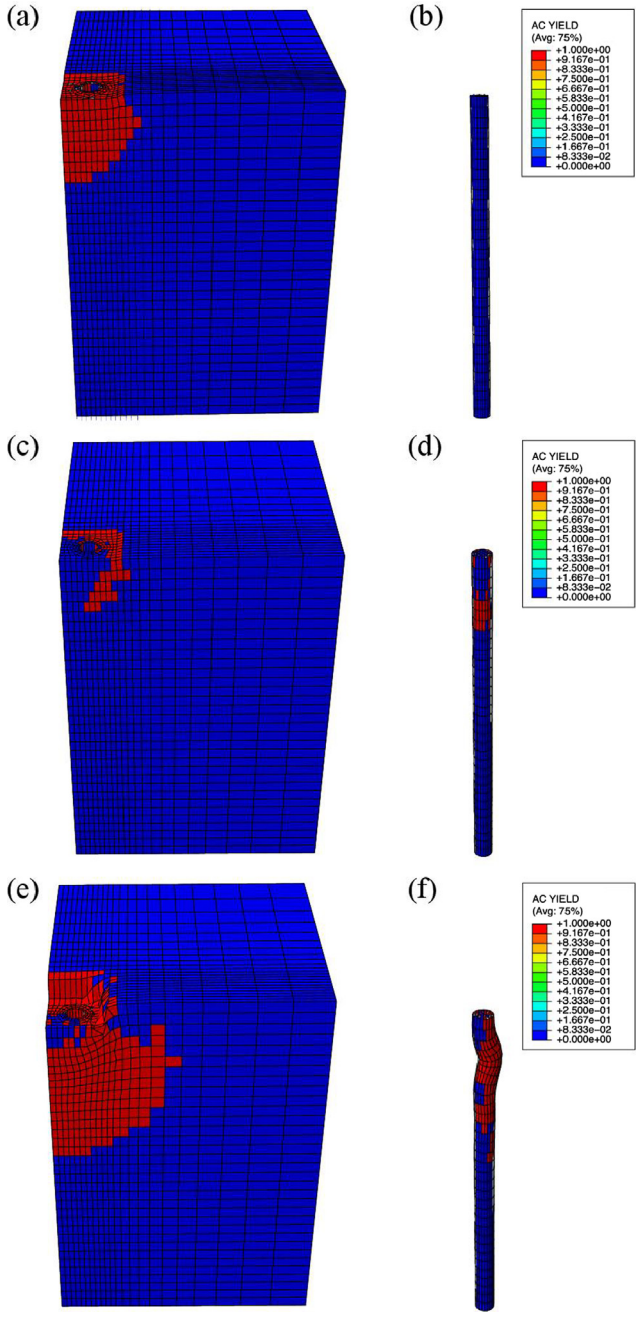

Fig. 11. Contours of zones of shear failure: (a) yield zones in soils under pressure at an applied stress of 120 kPa, (b) yield zones in column under pressure at an applied stress of 120 kPa, (c) yield zones in soils under embankment fill 1 at an applied stress of 140 kPa, (d) yield zones in column under embankment fill 1 at an applied stress of 140 kPa, (e) yield zones in soils under embankment fill 1 at an applied stress of 160 kPa, and (f) yield zones in column under embankment fill 1 at an applied stress of 160 kPa.

case under rigid footing or embankment fill, i.e., column failure occurs before soil failure, which is consistent with the observations from the model-scale laboratory tests.

The hyperbolic curve tangent modulus equation, proposed by Li (2008), was used to interpret the ultimate bearing capacity, q_{cs}, from the stress-settlement curve. The variations in q_{cs} with the area replacement ratio, m, are plotted in Fig. 12 for four cases under soft clay, embankment fill 1, embankment fill 2, and rigid footing. It should be emphasized that the results of q_{cs} for the cases of soft clay and ideal flexible pressure are similar, and that the outcomes of q_{cs} for the cases of rigid footing and embankment fill are close to each other, demonstrating that the influence of the foundation/fills on q_{cs} is not significant when the behavior of the composite ground is controlled by a certain failure mode. In general, the q_{cs} value increases monotonically with the m value. For the case of soft clay or ideal flexible pressure, the q_{cs} value does not change much with the column strength (q_u), whereas the q_{cs} value is improved when the soil strength (c_u) becomes higher. For the case of rigid footing or embankment fill, both higher column strength (q_u) and higher soil strength (c_u) can result in an increased q_{cs} value. This is because the failure pattern of composite grounds is controlled by soil failure or column failure for the case of soft clay and ideal flexible pressure or the case of rigid footing and embankment fill, respectively.

4. Discussions

4.1. Explanation of failure mechanism of composite ground using arching models

Compared to the rigid footing case, all composite grounds under earth fills show the development of soil-column differential settlement, which results in the occurrence of load transfer between the soil and the column in the soil-column system. The column has higher stiffness than the surrounding soil, which attracts more loads (the so-called negative arching effect) (Han et al., 2017; King et al., 2017; Zhang et al., 2018). A soil arching ratio, n, is defined as the ratio of the soil stress, σ_s, over the column stress, σ_c, to evaluate the load transfer mechanism. Han et al. (2017) modified the ground reaction curve (GRC) of Iglesia et al. (2014) using three segmented lines. Rui et al. (2018) distinguished two soil arching modes: the equal settlement (ES) pattern and the tower-shaped evolution (TSE) pattern. The minimum n value is often mobilized at a normalized displacement (differential settlement over clear spacing between columns) within the range of 0.6–1.7%, and the ultimate n value occurs at a normalized displacement of about 5–10% (Han et al., 2017). It should be noted that the models of Han et al. (2017) and Rui et al. (2018) were both developed for composite grounds under embankment fill, where column failure governs the design. Therefore, for all corresponding configurations of composite grounds in the numerical parametric analysis, the soil arching ratios are derived using the three models as shown in Fig. 13. The soil stress at the center, between the four columns, can be measured in the numerical model for comparing with the calculated column stress to derive the soil arching ratios. Fig. 13 indicates that the analytical and numerical calculations are generally in reasonable agreement. Liu (2003) stated that the n value falls within the

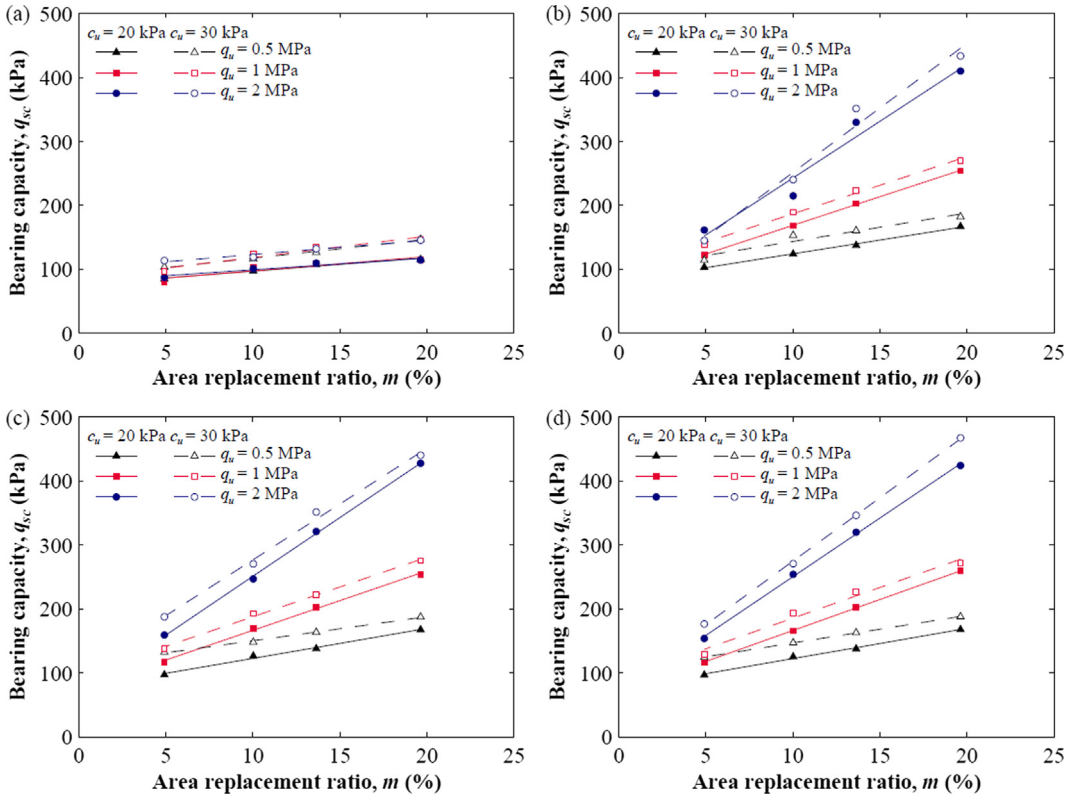

Fig. 12. Correlation between bearing capacity of composite ground and area replacement ratio under (a) soft clay, (b) embankment fill 1, (c) embankment fill 2, and (d) rigid footing.

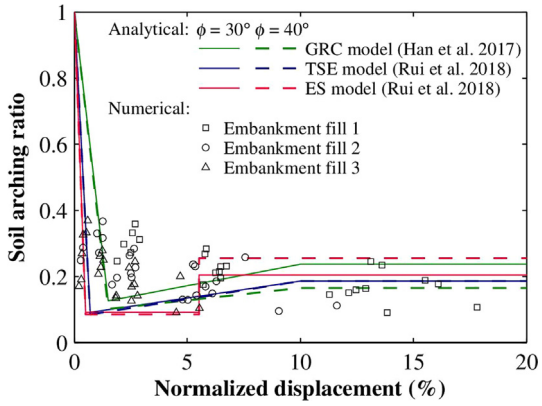

Fig. 13. Comparison of soil arching ratio obtained from numerical analyses and analytical models.

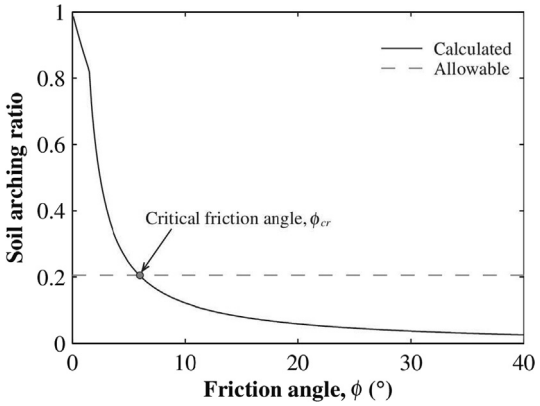

Fig. 14. Calculation example of critical friction angle ϕ_{cr} for the occurrence of column failure prior to soil failure for a case with a fill height of $H = 7$ m, supported by columns with a diameter of $D = 0.5$ m, an area replacement ratio of $m = 10.0\%$, and a strength of $q_u = 0.5$ MPa in soft soils with an undrained shear strength of $c_u = 20$ kPa.

range from 0.12 to 0.27 in the field tests, and within the range from 0.15 to 0.31 in different theoretical calculations. The results of the present numerical parametric study are also consistent with the suggestions of Liu (2003).

The ultimate bearing capacity of clayey soil can be calculated by $q_s = 5.14 \cdot c_u$ based on the Skempton (1951) bearing capacity factor of 5.14, whereas the ultimate bearing capacity of a fully penetrating uniform long column can be derived from its strength by $q_c = q_u$. Therefore, the ratio of $q_s/q_c = 5.14 \cdot c_u/q_u$ can be compared with the soil arching ratio to evaluate the critical proportion of the stresses shared by the soil and the column. If q_s/q_c is less than the soil arching ratio, more loads are taken by the column, which can result in the dominant mode of column failure. Otherwise, if q_s/q_c is greater than the soil arching ratio, soil failure controls the behavior of the composite ground. Using the three segmented GRC models of Han et al. (2017), Fig. 14 shows the correlation between the soil arching ratio and the friction angle of embankment fill for the case with a fill height of 7 m, supported by columns with

an area replacement ratio of $m = 10.0\%$ and a strength of $q_u = 1.0$ MPa in soft soils with an undrained shear strength of $c_u = 20$ kPa. In this case, the critical soil-column stress ratio is computed as $q_s/q_c = 5.14{\cdot}c_u/q_u = 0.21$, based on which the critical friction angle is calculated as $\phi_{cr} = 6°$. Hence, if the friction angle of the embankment fill is smaller than critical friction angle ϕ_{cr}, the surrounding soil takes more loads, leading to the occurrence of soil failure prior to column failure. In practice, however, the friction angle of the embankment fill is usually much higher than $\phi_{cr} = 6°$, which renders that column failure always occurs first for composite grounds under embankment fill.

The relation between ϕ_{cr} and fill height H is plotted in Fig. 15 for different combinations of q_u, c_u, and m. It should be noted that the bearing capacity of the untreated ground is $q_s = 5.14{\cdot}c_u$ and that soil failure never occurs when the fill height is less than a value of $H_{\min} = q_s/\gamma$, where γ is the unit weight of the earth fills ($\gamma = 20$ kN/m^3 in this investigation). Hence, in Fig. 15, the correlation between ϕ_{cr} and H starts from the $H_{\min}$ value. With the increase in H, the ϕ_{cr} value decreases nonlinearly. When the column has a lower strength (lower q_u), or the surrounding soil becomes more competent (higher c_u), the ϕ_{cr} value decreases, indicating that it becomes easier to trigger the occurrence of column failure prior to soil failure. Among all the calculated cases, the ϕ_{cr} value obtained from the case with $m = 4.9\%$, $c_u = 20$ kPa, and $q_u = 2$ MPa is the highest. In this case, the calculated bearing capacity of the composite ground is more than $q_{cs} = 160$ kPa, which corresponds to a fill height of $H = 8$ m and yields a critical friction angle of about $\phi_{cr} = 17°$. For commonly used soil and column parameters, one can see that it is very easy to mobilize the column strength rather than to trigger the occurrence of soil failure, since the ϕ_{cr} value is low in most cases (being less than 17°). Table 2 shows that the friction angle of embankment fill is generally higher than 30° in practice. The calculations demonstrate that the behavior of a composite ground under embankment fill is always governed by column failure, regardless of the compacted state of the embankment fill. In practice, Eq. (2) can be used to simplify Eq. (1) with $\lambda = 1.0$ and $\beta < 1.0$ for the composite ground under embankment fill.

It should be emphasized that most soil arching models were developed for embankment fill using effective shear strength parameters (Terzaghi et al., 1996; Iglesia et al., 2011; Zhuang et al., 2012; Han et al., 2017). When soft clay or dredged slurry is used as the fill material, the behavior of the soft fill is close to that of fluid. Hence, minimal negative soil arching effect can be mobilized in soft fills, leading to much less load transfer between soil prisms above the columns. The soil stress and the column stress are approximately equal, which can easily result in the occurrence of soil failure (i.e., $5.14{\cdot}c_u < q_u$). Therefore, the behavior of composite grounds under soft fills is governed by soil failure all the time.

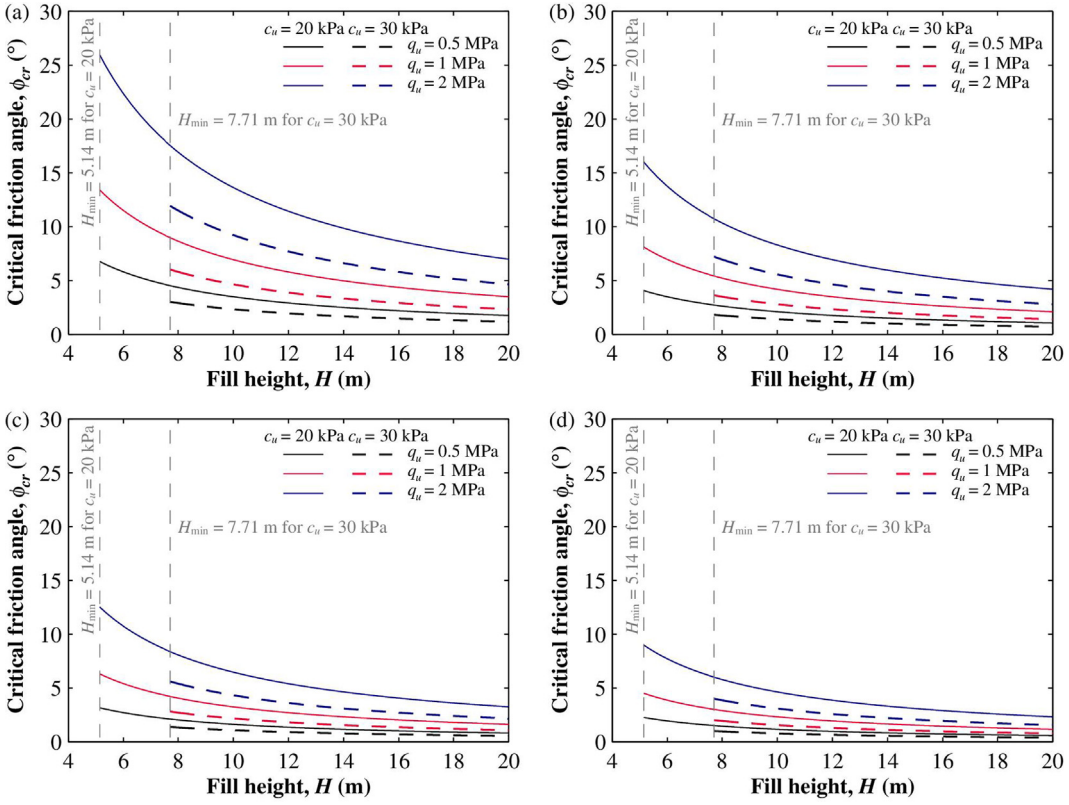

Fig. 15. Correlation of critical friction angle ϕ_{cr} with fill height H: (a) $m = 4.9\%$, (b) $m = 10.0\%$, (c) $m = 13.6\%$, and (d) $m = 19.6\%$.

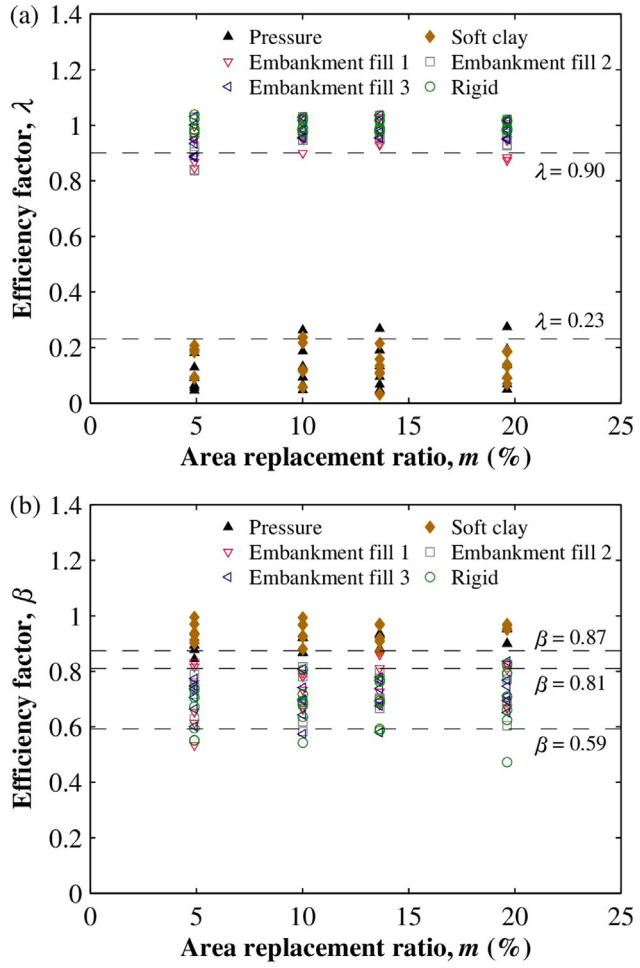

Fig. 16. Correlation between bearing capacity efficiency factors and area replacement ratio: (a) single column, λ, and (b) soils between columns, β.

4.2. Bearing capacity efficiency factors

Different arching models do not provide direct guidance on the calculation of bearing capacity efficiency factors for both the column and the soil (λ and β). In the JGJ 79 (2012) design guidelines, two factors, λ and β, are critical to determining the ultimate bearing capacity of a composite ground, and it is suggested that they can be estimated empirically based on local engineering experiences. In the numerical model, the mobilized column stress can be obtained directly, which can be compared against the column strength, q_u, to evaluate the λ value. Using Eq. (1), the β value can be derived based on the correlation among q_{cs}, column stress m, and $q_s = 5.14{\cdot}c_u$. Fig. 16 presents the correlations between the bearing capacity efficiency factors and the area replacement ratio for all 144 numerical analyses. Two scenarios should be distinguished for the case of a composite ground under soft clay and ideal flexible pressure or the case under embankment fill, as the failure mode differs. Under embankment fill, the 10th percentile (i.e., 10% of the data points are below that value) λ value is 0.90, and most β values fall within the range between the 10th percentile of 0.59 and the 90th percentile (i.e., 90% of the data points are below that value) of 0.81. This is similar to the recommendation in JGJ 79 (2012) for composite grounds under rigid footing. Hence, the design of composite grounds with soil-cement columns under embankment fill can also use Eq. (2) to simplify Eq. (1) with $\lambda = 1.0$ and $\beta < 1.0$. Under soft clay and ideal flexible pressure, the 90th percentile λ value is calculated as 0.23, and the 10th percentile β value is determined as 0.87. In this case, the full soil strength can be easily mobilized, and the choice of $\lambda < 1.0$ and $\beta = 1.0$ can be used in Eq. (1) during design for simplicity.

5. Conclusions

The main findings of this study are summarized below:

(a) The failure mechanisms of composite grounds under soft and embankment fills are different. Under soft fills, soil failure occurs first, whereas, under embankment fill, column failure primarily governs the response, which is similar to that under rigid footing.
(b) Under soft fills, the bearing capacity, q_{cs}, of composite grounds is proportional to the soil strength, c_u, but not the column strength, q_u, whilst, under embankment fill, q_{cs} increases with both q_u and c_u.
(c) Under embankment fill, the critical friction angle of earth fills can be derived based on the soil arching ratio, above which column failure always occurs prior to soil failure. The critical friction angle decreases with the fill height, and is often much lower than the friction angle for commonly used embankment fill materials.
(d) The bearing capacity efficiency factors for the column and the soil of composite grounds are derived for different types of earth fills. The behavior of a composite ground under embankment fill is close to the scenario under rigid footing, leading to $\lambda = 1.0$ and $\beta < 1.0$, whereas, under soft fills, the design should use $\lambda < 1.0$ and $\beta = 1.0$.

Acknowledgement

The research grant (M4081914.030) provided by Nanyang Technological University, Singapore, is highly appreciated.

References

Abusharar, S.W., Zheng, J.-J., Chen, B.-G., 2009. Finite element modeling of the consolidation behavior of multi-column supported road embankment. Comput. Geotech. 36 (4), 676–685.
Bergado, D., Lorenzo, G., 2002. Recent developments of ground improvement in soft Bangkok clay. Proceedings of the International Symposium on Lowland Technology. Saga University, Japan, pp. 17–26.
Bruce, D.A., 2001. Practitioner's guide to the deep mixing method. Proc. Instit. Civil Eng.-Ground Improvement 5 (3), 95–100.
Chai, J.-C., Shrestha, S., Hino, T., Ding, W.-Q., Kamo, Y., Carter, J., 2015. 2D and 3D analyses of an embankment on clay improved by soil–cement columns. Comput. Geotech. 68, 28–37.

Chai, J.-C., Shrestha, S., Hino, T., Uchikoshi, T., 2017. Predicting bending failure of CDM columns under embankment loading. Comput. Geotech. 91, 169–178.
Das, B.M., 2010. Geotechnical Engineering Handbook. J. Ross Publishing.
Gong, X.N., 2007. Generalized composite foundation theory and engineering application. Chinese J. Geotech. Eng. 29 (1), 1–13.
Han, J., Gabr, M., 2002. Numerical analysis of geosynthetic-reinforced and pile-supported earth platforms over soft soil. J. Geotech. Geoenviron. Eng. 128 (1), 44–53.
Han, J., Oztoprak, S., Parsons, R.L., Huang, J., 2007. Numerical analysis of foundation columns to support widening of embankments. Comput. Geotech. 34 (6), 435–448.
Han, J., Wang, F., Al-Naddaf, M., Xu, C., 2017. Progressive development of two-dimensional soil arching with displacement. Int. J. Geomech. 17 (12), 04017112.
Horpibulsuk, S., Chinkulkijniwat, A., Cholphatsorn, A., Suebsuk, J., Liu, M., 2012. Consolidation behavior of soil–cement column improved ground. Comput. Geotech. 43, 37–50.
Horpibulsuk, S., Miura, N., Bergado, D., 2004. Undrained shear behavior of cement admixed clay at high water content. J. Geotech. Geoenviron. Eng. 130 (10), 1096–1105.
Huang, J., Han, J., 2009. 3D coupled mechanical and hydraulic modeling of a geosynthetic-reinforced deep mixed column-supported embankment. Geotext. Geomembr. 27 (4), 272–280.
Iglesia, G.R., Einstein, H.H., Whitman, R.V., 2011. Validation of centrifuge model scaling for soil systems via trapdoor tests. J. Geotech. Geoenviron. Eng. 137 (11), 1075–1089.
Iglesia, G.R., Einstein, H.H., Whitman, R.V., 2014. Investigation of soil arching with centrifuge tests. J. Geotech. Geoenviron. Eng. 140 (2), 04013005.
Jamsawang, P., Voottipruex, P., Boathong, P., Mairaing, W., Horpibulsuk, S., 2015. Three-dimensional numerical investigation on lateral movement and factor of safety of slopes stabilized with deep cement mixing column rows. Eng. Geol. 188, 159–167.
JGJ 79. 2012. Technical code ground treatment of buildings. Edited by Ministry of Housing and Urban-Rural Development of the People's Republic of China. China Architecture & Building Press, Beijing.
King, D.J., Bouazza, A., Gniel, J.R., Rowe, R.K., Bui, H.H., 2017. Serviceability design for geosynthetic reinforced column supported embankments. Geotext. Geomembr. 45 (4), 261–279.
Kitazume, M., Terashi, M., 2013. The deep mixing method. CRC Press/Balkema, Leiden.
Li, R.-P., 2008. Nonlinear ground settlement calculated by hyperbolic curve tangent modulus equation. Rock Soil Mech. 29 (7), 1987–1992.
Liu, J., 2003. Analysis of pile-soil stress ratio for composite ground under embankment. Chinese J. Rock Mech. Eng. 22 (4), 674–677.
Liu, S.-Y., Du, Y.-J., Yi, Y.-L., Puppala, A.J., 2012. Field investigations on performance of T-shaped deep mixed soil cement column–supported embankments over soft ground. J. Geotech. Geoenviron. Eng. 138 (6), 718–727.
Lorenzo, G.A., Bergado, D.T., 2006. Fundamental characteristics of cement-admixed clay in deep mixing. J. Mater. Civ. Eng. 18 (2), 161–174.
Nunez, M., Briançon, L., Dias, D., 2013. Analyses of a pile-supported embankment over soft clay: Full-scale experiment, analytical and numerical approaches. Eng. Geol. 153, 53–67.
Rowe, R.K., Liu, K.-W., 2015. Three-dimensional finite element modelling of a full-scale geosynthetic-reinforced, pile-supported embankment. Can. Geotech. J. 52 (12), 2041–2054.
Rui, R., van Tol, F., Xia, Y.-Y., van Eekelen, S., Hu, G., 2018. Evolution of soil arching: 2D analytical models. Int. J. Geomech. 18 (6), 04018056.
Shen, S.-L., Han, J., Du, Y.-J., 2008. Deep mixing induced property changes in surrounding sensitive marine clays. J. Geotech. Geoenviron. Eng. 134 (6), 845–854.
Shen, S.-L., Miura, N., Koga, H., 2003. Interaction mechanism between deep mixing column and surrounding clay during installation. Can. Geotech. J. 40 (2), 293–307.
Shen, S.-L., Wang, Z.-F., Yang, J., Ho, C.-E., 2013. Generalized approach for prediction of jet grout column diameter. J. Geotech. Geoenviron. Eng. 139 (12), 2060–2069.
Shen, S.L., Chai, J.C., Miura, N., 2001. Stress distribution in composite ground of column-slab system under road pavement. First Asian-Pacific Congress on Computational Mechanics. Elsevier Science, Amsterdam, pp. 485–490.
Shen, S.L., Wang, Z.F., Cheng, W.C., 2017. Estimation of lateral displacement induced by jet grouting in clayey soils. Géotechnique 67 (7), 621–630.
Skempton, A.W., 1951. The bearing capacity of clays. Build. Res. Congr. 1, 180–189.
Talesnick, M., 2013. Measuring soil pressure within a soil mass. Can. Geotech. J. 50 (7), 716–722.
Terzaghi, K., Peck, R.B., Mesri, G., 1996. Soil mechanics in engineering practice. John Wiley & Sons.
Voottipruex, P., Bergado, D., Suksawat, T., Jamsawang, P., Cheang, W., 2011. Behavior and simulation of deep cement mixing (DCM) and stiffened deep cement mixing (SDCM) piles under full scale loading. Soils Found. 51 (2), 307–320.
Wang, Z.-F., Shen, S.-L., Modoni, G., 2019. Enhancing discharge of spoil to mitigate disturbance induced by horizontal jet grouting in clayey soil: Theoretical model and application. Comput. Geotech. 111, 222–228.
Wu, H., 2000. Analysis of composite foundation with rigid or flexible base slab Ph.D. thesis. Zhejiang University, Hangzhou, Zhejiang, China.
Xiao, H.W., Lee, F.H., Chin, K.G., 2014. Yielding of cement-treated marine clay. Soils Found. 54 (3), 488–501.
Yapage, N., Liyanapathirana, D., Kelly, R.B., Poulos, H.G., Leo, C.J., 2014. Numerical modeling of an embankment over soft ground improved with deep cement mixed columns: case history. J. Geotech. Geoenviron. Eng. 140 (11), 04014062.
Yapage, N., Liyanapathirana, D., Poulos, H.G., Kelly, R.B., Leo, C.J., 2015. Numerical modeling of geotextile-reinforced embankments over deep cement mixed columns incorporating strain-softening behavior of columns. Int. J. Geomech. 15 (2), 04014047.
Ye, G.B., Zhang, Z., Xing, H.F., Huang, M.S., Xu, C., 2012. Consolidation of a composite foundation with soil–cement columns and prefabricated vertical drains. Bull. Eng. Geol. Environ. 71 (1), 87–98.
Yi, Y., Li, C., Liu, S., Al-Tabbaa, A., 2014. Resistance of MgO-GGBS and CS-GGBS stabilised marine soft clays to sodium sulfate attack. Geotechnique 64 (8), 673–679.
Yi, Y., Liu, S., Puppala, A.J., 2016. Laboratory modelling of T-shaped soil–cement column for soft ground treatment under embankment. Géotechnique 66 (1), 85–89.
Yi, Y., Liu, S., Puppala, A.J., 2018. Bearing capacity of composite foundation consisting of T-shaped soil-cement column and soft clay. Transp. Geotech. 15, 47–56.
Yi, Y., Liu, S., Puppala, A.J., Jing, F., 2019. Variable-diameter deep mixing column for multi-layered soft ground improvement: Laboratory modeling and field application. Soils Found. 59 (3), 633–643.
Yi, Y., Liu, S., Puppala, A.J., Xi, P., 2017. Vertical bearing capacity behaviour of single T-shaped soil–cement column in soft ground: laboratory modelling, field test, and calculation. Acta Geotech. 12 (5), 1077–1088.
Yu, Y., Bathurst, R.J., Damians, I.P., 2016. Modified unit cell approach for modelling geosynthetic-reinforced column-supported embankments. Geotext. Geomembr. 44 (3), 332–343.
Zhang, L., Zhou, S., Zhao, H., Deng, Y., 2018. Performance of geosynthetic-reinforced and pile-supported embankment with consideration of soil arching. J. Eng. Mech. 144 (12), 06018005.
Zhuang, Y., Ellis, E., Yu, H., 2012. Three-dimensional finite-element analysis of arching in a piled embankment. Géotechnique 62 (12), 1127–1131.
Zhuang, Y., Wang, K., 2018. Finite-element analysis of arching in highway piled embankments subjected to moving vehicle loads. Géotechnique 68 (10), 857–868.